Article

Quantum Sieving Effect of Three-Dimensional Cu-Based Organic Framework for H and D

Daisuke Noguchi, Hideki Tanaka, Atsushi Kondo, Hiroshi Kajiro, Hiroshi Noguchi, Tomonori Ohba, Hirofumi Kanoh, and Katsumi Kaneko

J. Am. Chem. Soc., **2008**, 130 (20), 6367-6372 • DOI: 10.1021/ja077469f • Publication Date (Web): 30 April 2008

Snapshots of H_2 (a) and D_2 (b) on CuBOTf

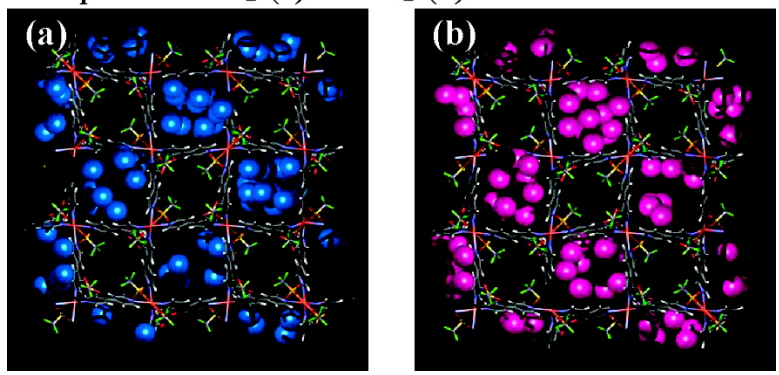

J|A|C|S
ARTICLES

Published on Web 04/30/2008

Quantum Sieving Effect of Three-Dimensional Cu-Based Organic Framework for H_2 and D_2

Daisuke Noguchi,[†] Hideki Tanaka,[‡] Atsushi Kondo,[†] Hiroshi Kajiro,[§] Hiroshi Noguchi,[†] Tomonori Ohba,[†] Hirofumi Kanoh,[†] and Katsumi Kaneko*[,†]

Department of Chemistry, Graduate School of Science, Chiba University, 1-33 Yayoi, Inage, Chiba, 263-8522, Japan, Department of Chemical Engineering, Graduate School of Engineering, Kyoto University, Nishikyo, Kyoto, 615-8510, Japan, and Nippon Steel Corporation, 20-1 Shintomi, Futtsu, Chiba, 293-8511 Japan

Received September 27, 2007; E-mail: kaneko@pchem2.s.chiba-u.ac.jp

Abstract: The crystal structure of $[Cu(4,4'\text{-bipyridine})_2(CF_3SO_3)_2]_n$ metal-organic framework (CuBOTf) of one-dimensional pore networks after pre-evacuation at 383 K was determined with synchrotron X-ray powder diffraction measurement. Effective nanoporosity of the pre-evacuated CuBOTf was determined with N_2 adsorption at 77 K. The experimental H_2 and D_2 adsorption isotherms of CuBOTf at 40 and 77 K were measured and then compared with GCMC-simulated isotherms using the effective nanoporosity. The quantum-simulated H_2 and D_2 isotherms at 77 K using the Feynman−Hibbs effective potential coincided with the experimental ones, giving a direct evidence on the quantum molecular sieving effect for adsorption of H_2 and D_2 on CuBOTf. However, the selectivity for the 1:1 mixed gas of H_2 and D_2 was 1.2. On the contrary, experimental H_2 and D_2 isotherms at 40 K had an explicit adsorption hysteresis, originating from the marked pore blocking effect on measuring the adsorption branch. The blocking effect for quantum H_2 is more prominent than that for quantum D_2; the selectivity for D_2 over H_2 at 40 K was in the range of 2.6 to 5.8. The possibility of the quantum molecular sieving effect for H_2 and D_2 adsorption on $[Cu_3(\text{benzene-1,3,5-tricarboxylate})_2(H_2O)_3]_n$ of three-dimensional pore networks was also shown at 77 K.

Introduction

The global warming effect has given a critical warning to human beings. Therefore, chemistry has focused on developing highly efficient chemical technologies to reduce energy consumptions and emissions. The intensive research on nanoporous materials, being key materials to realize environmentally friendly technology, has been accelerated by worldwide demands. Zeolites, activated carbons, and porous glasses are representatives of traditional nanoporous materials that have been widely used in various technologies.[1] New nanoporous materials of hopeful applicants for highly efficient chemical technologies are classified into three groups; single-walled nanocarbons such as single-walled carbon nanotubes (SWCNTs),[2,3] mesoporous silicas of a well-ordered pore structure such as MCM-41,[4] and metal-organic frameworks (MOFs).[5,6] The mesoporous silicas have larger nanopores than the other two groups, which have been tried to be applied to catalysis and separation engineerings. Nanocarbons of high electrical conductivity and great stability have been actively studied for energy storage and sensors. The MOFs are not thermally stable compared with other two groups. On the contrary, the nanopore structure of the MOF can be designed and synthesized according to a specific application.[7–15] That is, the MOF can have great potential applications. One hopeful application is on clean energy storage materials. Many papers on hydrogen and methane adsorption on MOFs have been published, stimulating science and technologies.[16–34] The great feature of the MOFs for gas storage is an inherent structure

[†] Chiba University.
[‡] Kyoto University.
[§] Nippon Steel Corporation.

(1) Llewellyn, P. L., Rodriguez-Reinoso, F.; Rouqerol, J.; Seaton, N. *Characterization of Porous Solids VII*; Elsevier: New York, 2007.
(2) Iijima, S.; Ichihashi, T. *Nature* **1993**, *363*, 603–605.
(3) Bethune, D. S.; Kiang, D. H.; de Vries, M. S.; Gorman, G.; Savoy, R.; Vazquez, J.; Beyers, R. *Nature* **1993**, *363*, 605–607.
(4) Kapoor, P.; Inagaki, S.; Ikeda, S.; Kakiuchi, K.; Suda, M.; Shimada, T. *J. Am. Chem. Soc.* **2005**, *127*, 8174–8178.
(5) Eddaoudi, M.; Moler, D. B.; Li, H.; Chen, B.; Reineke, T. M.; O'Keeffe, M.; Yaghi, O. M. *Acc. Chem. Res.* **2001**, *34*, 319–330.
(6) Eddaoudi, M.; Kim, J.; Rosi, N.; Vodak, D.; Wachter, J.; O'Keeffe, M.; Yaghi, O. M. *Science* **2002**, *295*, 469–472.
(7) Hoskins, B. F.; Robson, R. *J. Am. Chem. Soc.* **1990**, *112*, 1546–1554.
(8) Batten, S. R.; Robson, R. *Angew. Chem., Int. Ed.* **1998**, *37*, 1460–1494.
(9) Khlobstov, A. N.; Blake, A. J.; Champness, N. R.; Lemenovskii, D. A.; Majouga, A. G.; Zyk, N. V.; Schröder, M. *Coord. Chem. Rev.* **2001**, *222*, 155–192.
(10) Carlucci, L.; Ciani, G.; Proserpio, D. M. *J. Chem. Soc., Dalton Trans.* **1999**, 1799–1804.
(11) Chui, S. S.-Y.; Lo, S. M.-F.; Charmant, J. P. H.; Orpen, A. G.; Williams, I. D. *Science* **1999**, *283*, 1148–1150.
(12) Barnett, S. A.; Champness, N. R. *Coord. Chem. Rev.* **2003**, *246*, 145–168.
(13) Kitagawa, S.; Kitaura, R.; Noro, S. *Angew. Chem., Int. Ed.* **2004**, *43*, 2334–2375.
(14) Férey, G.; Mellot-Draznieks, C.; Serre, C.; Millange, F. *Acc. Chem. Res.* **2005**, *38*, 217–225.
(15) Bradshaw, D.; Claridge, J. B.; Cussen, E. J.; Prior, T. J.; Rosseinsky, M. J. *Acc. Chem. Res.* **2005**, *38*, 273–282.
(16) Kondo, M.; Shimamura, M.; Noro, S.; Minakoshi, S.; Asami, A.; Seki, K.; Kitagawa, S. *Chem. Mater.* **2000**, *12*, 1288–1299.
(17) Kitaura, R.; Seki, K.; Akiyama, G.; Kitagawa, S. *Angew. Chem., Int. Ed.* **2003**, *42*, 428–431.
(18) Rosi, N. L.; Eckert, J.; Eddaoudi, M.; Vodak, D. T.; Kim, J.; O'Keeffe, M.; Yaghi, O. M. *Science* **2004**, *300*, 1127–1129.

flexibility, which can accommodate molecules to form a new clathrate lattice. Kondo et al. showed that a Cu-based MOF expands the *c*-axis by 30% on CO_2 adsorption.[35] As the absolute storage amount of MOFs for supercritical hydrogen is not necessarily larger than that of nanoporous carbons, a new application potential of the MOFs must be examined. Separation of a valuable substance is one of basic technologies. Zeolites and carbon molecular sieves have contributed to modern technologies such as air separation; these nanoporous materials are effective for separation of molecules having different size and shape.[36] Consequently, isotopic separation for H_2 and D_2, for example, cannot be done by these traditional molecular sieving materials. Johnson et al. developed quantum molecular sieving effect of SWCNT for the isotopic separation with path integral method[37–39] on the basis of the hard sphere model by Beenakker et al.[40] They showed the possibility that the bundled SWCNT gives a high selectivity for T_2 over H_2 at 20 K. Tanaka et al. evidenced experimentally the quantum molecular sieving effect for H_2 and D_2 using single wall carbon nanohorns through measuring of equilibrium adsorption isotherms.[41–43] The additional experimental evidence on the quantum molecular sieving effect for nanoporous carbons have been published recently.[44] Furthermore, a theoretical study by Kumar et al.[45,46] showed the possibility of the quantum molecular sieving for H_2 and D_2 due to their marked diffusion difference. Some experimental kinetic molecular sieving has been presented recently.[47,48] Therefore, we need to study the quantum molecular sieving effect on MOFs whose pore structure is highly tunable. At the first stage of the study, authors tried to get explicit evidence on the quantum molecular sieving effect for adsorption of H_2 and D_2 on MOF having a simple pore network structure with both of experimental and quantum simulation techniques. We chose$[Cu(4,4'\text{-bipyridine})_2(CF_3SO_3)_2]_n$(denoted as "CuBOTf" in this article) having one-dimensional nanopore channels for this research. $[Cu_3(\text{benzene-1,3,5-tricarboxolate})_2(H_2O)_3]_n$ (denoted as "Cu-BTC") of three-dimensional pore networks,[11] which exhibits high adsorptivity for supercritical H_2, was used for the experimental comparison.

Experimental Details and Simulation

We synthesized a large amount of CuBOTf powder (10 g in one batch) by the method described in the literature,[49] using tetrahydrofran as a solvent. The Cu-BTC powders were also synthesized for comparison after the procedure described in the literature,[11] because Cu-BTC exhibits a promising H_2 adsorptivity.[32] The crystal structure of the CuBOTf preheated at 383 K in vacuo was obtained using a synchrotron X-ray powder diffraction (XRPD) pattern at the Super Photon Ring (SPring-8, Hyogo, Japan). The XRPD pattern of the preheated CuBOTf powder was measured at room temperature with the radiation wavelength of 0.1001 nm. The structure analysis of CuBOTf was performed by a direct method using software EXPO2004.[50] The powder X-ray diffraction pattern of Cu-BTC crystals was collected on a X-ray diffractometer (RIGAKU, mini Flex) with Cu Kα radiation (30kV, 15mA).Thermogravimetric analyses (TGA) of the synthesized samples were performed under a nitrogen flow of 100−150 mL/min over a range of temperatures from ambient temperature to 773−1100 K at a heating rate of 3−5 K/min.

The nitrogen adsorption isotherm of CuBOTf was measured gravimetrically at 77 K after pretreatment at 383 K under 1 mPa for 2 h. The H_2 and D_2 adsorption isotherms of CuBOTf at 77 and 40 K were then measured with laboratory-designed volumetric adsorption equipment. The H_2 and D_2 adsorption isotherms of Cu-BTC were measured at 77 K using an automatic adsorption equipment (Autosorb-1, Quantachrome). All samples for H_2 and D_2 adsorption were outgassed under 1 mPa before each adsorption measurement (CuBOTf: 383 K for 5 h, Cu-BTC: 473 K for 2 h).

The grand canonical Monte Carlo (GCMC) simulation[51] was used to compute N_2, H_2, and D_2 adsorption isotherms of only CuBOTf, assuming that the CuBOTf has a rigid structure of one-dimensional pore networks at all temperatures. This is because the synchrotron X-ray diffraction patterns at room temperature and 77 K almost coincided with each other. In this study, we did not simulate the adsorption isotherms of Cu-BTC having three-dimensional pore networks. The Lennard-Jones (LJ) potential was used to model fluid-fluid interaction potentials:

(19) Rowsell, J. L. C.; Millward, A. R.; Park, K. S.; Yaghi, O. M. *J. Am. Chem. Soc.* **2004**, *126*, 5666–5667.
(20) Rowsell, J. L.; Yaghi, O. M. *J. Am. Chem. Soc.* **2006**, *128*, 1304–1315.
(21) Dybtsev, D. N.; Chun, H.; Yoon, S. H.; Kim, D.; Kim, K. *J. Am. Chem. Soc.* **2004**, *126*, 32–33.
(22) Pan, L.; Sander, M. B.; Huang, X.; Li, J.; Smith, M.; Bitttner, E.; Bockrath, B.; Johnson, J. K. *J. Am. Chem. Soc.* **2004**, *126*, 1308–1309.
(23) Noguchi, H.; Kondoh, A.; Hattori, Y.; Kanoh, H.; Kajiro, H.; Kaneko, K. *J. Phys. Chem. B* **2005**, *109*, 13851–13853.
(24) Panella, B.; Hirscher, M. *Adv. Mater.* **2005**, *17*, 538–541.
(25) Kesanli, B.; Cui, Y.; Smith, M. R.; Bittner, E. W.; Bockrath, B. C.; Lin, W. *Angew. Chem., Int. Ed.* **2004**, *44*, 72–75.
(26) Dailly, A.; Vajo, J. J.; Ahn, C. C. *J. Phys. Chem. B* **2006**, *110*, 1099–1101.
(27) Garberoglio, G.; Skoulidas, A. I.; Johnson, J. K. *J. Phys. Chem. B* **2005**, *109*, 13094–13103.
(28) Yang, Q.; Zhong, C. *J. Phys. Chem. B* **2005**, *109*, 11862–11864.
(29) Sagara, T.; Klassen, J.; Ganz, E. *J. Chem. Phys.* **2004**, *121*, 12543–12547.
(30) Skoulidas, A. I.; Sholl, D. S. *J. Phys. Chem. B* **2005**, *109*, 15760–15768.
(31) Mueller, T.; Ceder, G. *J. Phys. Chem. B* **2005**, *109*, 17974–17983.
(32) Panella, B.; Hirscher, M.; Pütter, H.; Müller, U. *Adv. Funct. Mater.* **2006**, *16*, 520–524.
(33) Collins, D. J.; Zhou, H.-C. *J. Mater. Chem.* **2007**, *17*, 3154–3160.
(34) Lin, X.; Blake, A. J.; Wilson, C.; Sun, X. Z.; Champness, N. R.; George, M. W.; Hubberstey, P.; Mokaya, R.; Schröder, M. A. *J. Am. Chem. Soc.* **2006**, *128*, 10745–10753.
(35) Kondo, A.; Noguchi, H.; Ohnishi, S.; Kajiro, H.; Tohdoh, A.; Hattori, Y.; Xu, W.; Tanaka, H.; Kanoh, H.; Kaneko, K. *Nano Lett.* **2006**, *6*, 2581–2584.
(36) Corma, A. *Chem. Rev.* **1997**, *97*, 2373–2419.
(37) Wang, Q.; Challa, S. R.; Sholl, D. S.; Johnson, J. K. *Phys. Rev. Lett.* **1999**, *82*, 956–959.
(38) Challa, S. R.; Sholl, D. S.; Johnson, J. K. *Phys. Rev. B* **2001**, *63*, 2454191–2454199.
(39) Challa, S. R.; Sholl, D. S.; Johnson, J. K. *J. Chem. Phys.* **2002**, *116*, 814–824.
(40) Beenakker, J. J. M.; Borman, V. D.; Krylov, S. Y. *Chem. Phys. Lett.* **1995**, *232*, 379–382.
(41) Tanaka, H.; Kanoh, H.; El-Merraoui, M.; Steele, W. A.; Yudasaka, M.; Iijima, S.; Kaneko, K. *J. Phys. Chem. B* **2004**, *108*, 17457–17465.
(42) Tanaka, H.; Kanoh, H.; Yudasaka, M.; Iijima, S.; Kaneko, K. *J. Am. Chem. Soc.* **2005**, *127*, 7511–7516.
(43) Tanaka, H.; Fan, J.; Kanoh, H.; Yudasaka, M.; Iijima, S.; Kaneko, K. *Mol. Simul.* **2005**, *31*, 465–474.
(44) Hattori, Y.; Tanaka, H.; Okino, F.; Touhara, H.; Nakahigashi, Y.; Utsumi, S.; Kanoh, H.; Kaneko, K. *J. Phys. Chem. B* **2006**, *110*, 9764–9767.
(45) Kumar, A. V. A.; Bhatia, S. K. *Phys. Rev. Lett.* **2005**, *95*, 245901.
(46) Kumar, A. V. A.; Jobic, H.; Bhatia, S. K. *J. Phys. Chem. B* **2006**, *110*, 16666–16671.
(47) Zhao, X.; Villar-Rodil, S.; Fletcher, A. J.; Thomas, K. M. *J. Phys. Chem. B* **2006**, *110*, 9947–9955.
(48) Chu, X. Z.; Zhou, Y. P.; Zhang, Y. Z.; Su, W.; Sun, Y.; Zhou, L. *J. Phys. Chem. B* **2006**, *110*, 22596–22600.
(49) Carlucci, L.; Cozzi, N.; Ciani, G.; Moret, M.; Proserpio, D. M.; Rizzato, S. *Chem. Commun.* **2002**, 1354–1355.
(50) Altomare, A.; Burla, M. C.; Camalli, M.; Carrozzini, B.; Cascarano, G. L.; Giacovazzo, C.; Guagliardi, A.; Moliterni, A. G. G.; Polidori, G.; Rizzi, R. *J. Appl. Crystallogr.* **1999**, *32*, 339–340.
(51) Allen, M. P., Tildesley, D. J., Eds. *Computer Simulation of Liquids*; Clarendon Press: Oxford, 1987),

$$V_{LJ}(r) = 4\varepsilon_{ff}\left[\left(\frac{\sigma_{ff}}{r}\right)^{12} - \left(\frac{\sigma_{ff}}{r}\right)^{6}\right] \quad (1)$$

where r is the distance between two molecules. N_2 and H_2 molecules were treated as a structureless spherical particle, and the LJ interaction parameters used in this work are $\sigma_{ff} = 0.3615$ nm and $\epsilon_{ff}/k_B = 101.5$ K for N_2,[52] and $\sigma_{ff} = 0.2958$ nm and $\epsilon_{ff}/k_B = 36.7$ K for H_2,[53,54] respectively. The same interaction parameters for H_2 were used for D_2. The Feynman−Hibbs (FH) effective potential[55,56] was used to introduce quantum effects in hydrogen isotope adsorption; the following quadratic FH effective potential[57] was used:

$$V_{FH}(r) = V_{LJ}(r) + \frac{\hbar^2}{24\mu k_B T}\left[V_{LJ}''(r) + \frac{2}{r}V_{LJ}'(r)\right] \quad (2)$$

where $\mu = m/2$ (m is mass of a quantum fluid molecule) is the reduced mass of a pair of interacting fluid molecules. The interaction potentials of an adsorbate molecule with the atoms in the CuBOTf framework were modeled by the all-atoms OPLS force field (OPLS-AA)[58,59] without any electrostatic interactions. The solid-fluid interaction parameters ϵ_{sf} and σ_{sf} were calculated by the Lorentz−Berthelot combining rules. The interaction potentials between a quantum H_2 (or D_2) molecule and the solid atoms in the CuBOTf framework were calculated by eq 2 replacing ϵ_{ff} and σ_{ff} with ϵ_{sf} and σ_{sf}, respectively, and assuming $\mu = m$.

The probabilities of a single displacement, creation, and deletion were set to 0.4, 0.3, and 0.3, respectively. The system was equilibrated for 2.5×10^7 Monte Carlo steps, after which data were collected for another 2.5×10^7 steps. The fluid−fluid and solid−fluid interactions were truncated at distances of 4.09 σ_{ff} and 4.09 σ_{sf}, respectively. Periodic boundary conditions were applied along the crystallographic a, b, and c axes. The GCMC simulations yield an absolute adsorbed amount (N_{abs}), and thus it must be converted to a surface excess adsorption (N_{exc}) for comparison with experimental data. In the present study, the surface excess adsorption was calculated by $N_{exc} = N_{abs} - \rho_b V$, where ρ_b is the bulk density of gas and V is the volume of the internal pore spaces of the CuBOTf framework. In the grand canonical ensemble, the volume, temperature, and adsorbate chemical potential are fixed, and thus we need to obtain the pressure of bulk fluid as a function of chemical potential at the same temperature to compare with experimental isotherms. In this study, we also performed Monte Carlo simulations with the FH effective potential in the canonical ensemble (FH-MC), which was combined with the Widom test particle insertion method[60] to determine excess chemical potentials of quantum hydrogen isotopes at 77 and 40 K. The pressures of quantum hydrogen isotopes were calculated simultaneously during the FH-MC simulations. As an H_2 molecule does not specifically interact with a D_2 molecule, ideal adsorption solution theory (IAST)[61] was applied to predict mixture adsorption isotherms for H_2 and D_2, leading to the selectivity $S(D_2/H_2)$ of D_2 over H_2. Details of calculation are shown in the Supporting Information.

Results and Discussion

The crystal structure of preheated CuBOTf (Figure 1) belongs to the tetragonal space group $P4_2nm$ (no. 102), $a = b =$ 1.9933(5) nm, $c = 0.9645(5)$ nm, $V = 3.83219$ nm^3, $M = 674.08$, $Z = 4$, and $\rho = 1.17$ g/cm^3 ($R_p = 0.0843$, $R_{wp} = 0.1463$). The fundamental framework structure consists of Cu(II) ions and 4,4′-bipyridine units forming a 3D framework of two identical interwoven nets of the topological type, which is similar to the framework previously reported.[49] It has nanoporous channels extending to the direction of the crystallographic c axis. The network topology of CuBOTf produces two types of the latter channels; one is limited by 2-fold entangled 4_1 helixes, while the other is simply formed by the stacking of the folded squares, and each has a square section (ca. 1.1×1.1 nm^2, in terms of center-to-center distance of Cu(II) ions) with a chessboard disposition. The structure of preheated CuBOTf is almost identical to that determined by Carlucci et al. at 204 K.[49] The cross sections of the 1D channels of the CuBOTf framework are 0.87×0.87 nm^2 and 0.20×0.20 nm^2, respectively. Here, the H_2 and N_2 molecules are adsorbed only in the large pores of the preheated CuBOTf framework because the molecular diameters of H_2 ($\sigma_{ff} = 0.2958$ nm) and N_2 ($\sigma_{ff} = 0.3615$ nm) are larger than the entrance of the small pore (0.20×0.20 nm^2). However, the low reliability factor of the X-ray diffraction analysis suggests orientational disorders of CF_3SO_3 anions in the preheated CuBOTf, indicating the pore blocking even for larger pores of 0.87 nm (Figure S1, Supporting Information). The X-ray powder diffraction pattern of synthesized Cu-BTC crystals which was used for comparison coincided with that in the literature (Figure S2, Supporting Information).[11] TGA curve of the CuBOTf sample showed a gradual weight loss from 300 K and it reached 10.2% at 473 K due to detachment of guest molecules in CuBOTf, and then the framework decomposes over a temperature ranges 550−700 K (Figure S3, Supporting Information). Therefore, in this study, we preheated CuBOTf at 383 K for gas adsorption experiments. The difference of sample weight (10.7%) before and after the preheating almost coincided with the weight loss by the detachment of guest molecules determined from the TGA data (10.2%). The TGA curve of synthesized Cu-BTC crystals showed over 20% of weight loss up to 383 K showing dehydration (Figure S4, Supporting Information).[11]

The experimental N_2 adsorption isotherm of preheated CuBOTf at 77 K (Figure S5, Supporting Information) is of type I, suggesting that the preheated CuBOTf is highly microporous. Simulated N_2 adsorption isotherms of the CuBOTf framework at 77 K is of type I isotherm. However, the experimental N_2

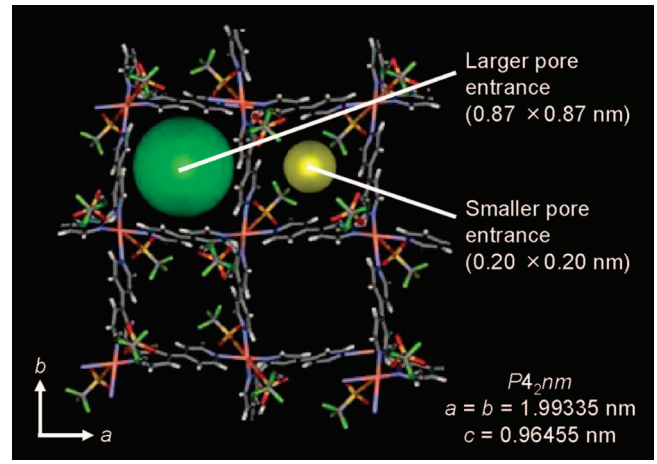

Figure 1. Schematic view of the frameworks of CuBOTf. Effective diameters of the pore entrances are shown with large spheres. (Brown: Cu; gray: C; blue: N: red; O: yellow; S: yellow green: F; white: H.)

(52) Neimark, A. V.; Ravikovitch, P. I.; Vishnyakov, A. *Phys. Rev. E.* **2000**, *62*, R1493–R1496.
(53) Darkrim, F.; Aoufi, A.; Levesque, D. *Mol. Simul.* **2000**, *24*, 51–61.
(54) Darkrim, F.; Levesque, D. *J. Phys. Chem. B* **2000**, *104*, 6773–6776.
(55) Feynman, R. P., Hibbs, A., Eds. *Quantum Mechanics and Path Integrals*; McGraw-Hill: New York, 1965.
(56) Feynman, R. P., Ed. *Statistical Mechanics*; W. A. Benjamin: Reading, MA, 1972.
(57) Sesé, L. M. *Mol. Phys.* **1996**, *89*, 1783–1802.
(58) Jorgensen, W. L.; Maxwell, D. S.; Tirado-Rives, J. *J. Am. Chem. Soc.* **1996**, *118*, 11225–11236.
(59) Watkins, E. K.; Jorgensen, W. L. *J. Phys. Chem. A* **2001**, *105*, 4118–4125.
(60) Widom, B. *J. Phys. Chem.* **1982**, *86*, 869–872.
(61) Myers, A. L.; Prausnitz, J. M. *AIChE J.* **1965**, *11*, 121–127.

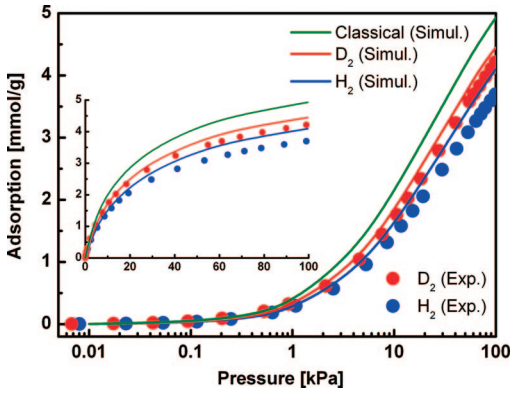

Figure 2. Simulated and experimental adsorption isotherms of CuBOTf for H_2 and D_2 at 77 K. The circles represent the experimental adsorption isotherms, while the lines represent the simulated isotherms from the CuBOTf model. Feynman−Hibbs effective potential is used for quantum simulation, while Lennard-Jones potential is used for classical simulation. The pressures are given in logarithmic (inset is in linear) scales.

adsorption amounts at $P/P_0 = 0.95$ is 0.618 times smaller than that from simulation. Here, the pore volume from the crystal structure was evaluated using a hydrogen atom of the van der Waals radius as the probe (PLATON Software) and the experimental pore volume was obtained assuming the liquid density of adsorbed N_2. As the adsorption isotherm simulated with GCMC is not affected by the pore blocking, the differences can most likely be ascribed to the pore narrowing due to the orientational disorders of CF_3SO_3 anions in the CuBOTf. Thus, only 0.618 of the pores in the CuBOTf sample is available for N_2 adsorption due to the pore narrowing. We therefore introduced an effective nanoporosity factor of 0.618 for the GCMC simulation.

The experimental and simulated adsorption isotherms of CuBOTf for H_2 and D_2 at 77 K (Figure 2) show that the experimental adsorbed amount of D_2 exceeds that of H_2 over a whole range of pressures by about 13% due to the quantum effects. Here, the reproducibility in the adsorption measurements of H_2 and D_2 were within 3% and thereby the observed difference between H_2 and D_2 is valuable. Moreover, classical simulation using LJ potential instead of FH effective potential for quantum simulation, gave the adsorption amounts which are greater than those for quantum H_2 and D_2 by 20%. This reveals that the quantum effects are essential for hydrogen isotope adsorption even at 77 K. The quantum simulation isotherms are in good agreement with the experimental isotherms for both H_2 and D_2; the predictions from the simulation coincided with experiments over a wide range of pressures without any refinements of the OPLS-AA force field, indicating that the potentials used are appropriate for modeling of the CuBOTf framework atoms. Although Cu-BTC has nanopores comparable to those of CuBOTf, the adsorption amount for D_2 was larger than that for H_2 at 77 K by 20%, being a more evident difference between D_2 and H_2 adsorption than CuBOTf (Figure S6, Supporting Information). This adsorption difference should stem from the quantum molecular sieving effect, indicating that marked quantum molecular sieving effect can be observed widely for many kinds of MOFs.

The potential energy contour of H_2 at 77 K is shown in Figure 3. In the larger pore of CuBOTf limited by 2-fold entangled 4_1 helixes along the *c* axis (Figure 3A and 3B), the corners near the Cu(II) ions give the largest interaction potential energy (Figure 3C and 3D). This adsorption process can be understood from configurational snapshots of adsorbed H_2 in CuBOTf at 77 K obtained from the simulations. The H_2 molecules start to be adsorbed at the corners of the 1D channels and the 4,4′-bipyridine units of CuBOTf at low pressures (Figure 3E), followed by the filling of H_2 molecules in the inner spaces of the pore at 100 kPa (Figure 3F).

Experimental and simulated adsorption isotherms of CuBOTf for H_2 and D_2 at 40 K are shown in Figure 4. Both experimental isotherms for H_2 and D_2 are representative of the Langmuir type, indicating an intensive molecule-pore wall interaction. It is evident that the adsorption amount of D_2 is larger than that of H_2 by 13% above 60 kPa, being similar to that at 77 K. The simulated isotherm of H_2 after the correction using the effective nanoporosity factor agrees well with the experimental isotherm of the desorption branch rather than the adsorption branch in the pressure range of 5 to 100 kPa. However, the experimental adsorption branch deviates seriously from the simulated isotherm below 50 kPa for H_2 and below 20 kPa for D_2. For example, the observed value is only 0.75 of the simulated value for H_2 at 5 kPa. The discrepancy between the simulation and experimental adsorption branches becomes considerable with the decrease of the H_2 pressure, although the discrepancy for D_2 is not as marked. Although the experimental desorption branches below 100 Pa are not determined due to the experimental difficulty, the discrepancy between the simulated and experimental isotherms should be inherent to the adsorption branch. The fact that desorption amount is larger than the adsorption amount in nanoporous systems is often attributed to an insufficient equilibration due to the limited diffusion of adsorptive molecules in small pores. Recently Skoulidas and Sholl reported that gas diffusion at room temperature depends on the gas loading, sort of gases, and pore structure for several MOF systems with molecular dynamics simulations.[62] Consequently, diffusion process should be even more important at low temperature in the nanopores of the CuBOTf.

Then we examine the effect of the equilibration time on adsorption. The H_2 adsorption amount measured at 3−6 h after a dose of H_2 gas was smaller than that at 6−12 h by 20% over the whole pressure range (Figure S7, Supporting Information). Accordingly, diffusion of quantum H_2 is suppressed by the narrow 1D nanopores. Recent theoretical studies on quantum molecular sieving for H_2 and D_2 by Kumar et al.[45,46] predict that the diffusion rate of quantum H_2 molecules is smaller than that of quantum D_2 molecules in nanopores of zeolites rho. The observed discrepancy between the simulated and experimental adsorption amounts in the low pressure region for H_2 and D_2 can be interpreted by the above-mentioned quantum diffusion effect. Certainly, the discrepancy for D_2 is not as marked as that for H_2, although the D_2 adsorption was measured at 2−3 h after introduction of D_2 gas (H_2 at 6−10 h). It is noteworthy that H_2 molecules behave as if they are greater in molecular size than D_2 molecules even in the diffusion process due to quantum effects. The isosteric heat of adsorption data also supports the presence of the quantum diffusion effect. The experimental q_{st} values determined from the adsorption branches at 40 and 77 K were 3 kJ mol^{-1} for H_2 and 4 kJ mol^{-1} for D_2, being smaller than the corresponding values from simulation (6.2 kJ mol^{-1} for H_2 and 6.4 kJ mol^{-1} for D_2) (Figure S8, Supporting Information). This discrepancy can be attributed to the experimental adsorption amount which is underestimated due to the very slow diffusion of quantum H_2 and D_2 at 40 K.

(62) Skoulidas, A. I.; Sholl, D. S. *J. Phys. Chem. B.* **2005**, *109*, 1576–15768.

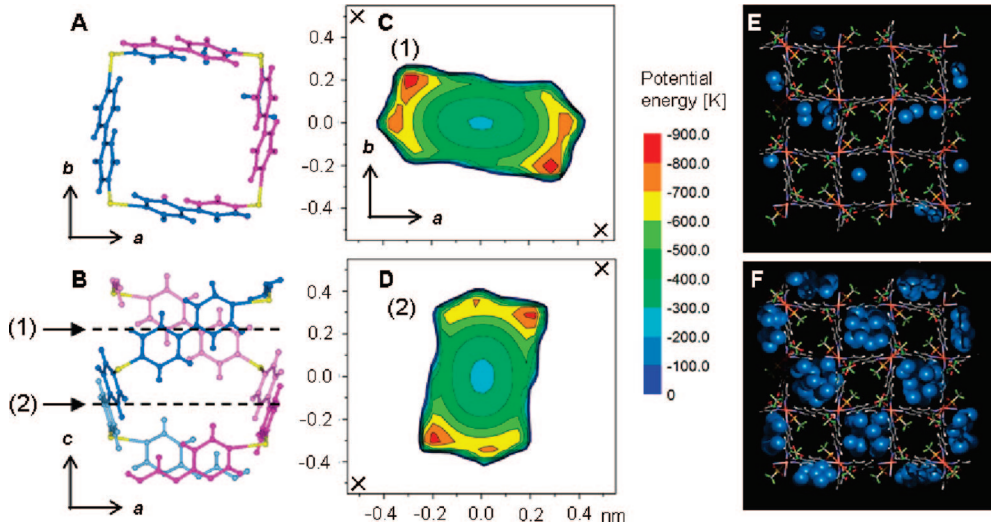

Figure 3. (A) Top view from the *c* axis and (B) side view from the *b* axis of the larger pore of CuBOTf model. (C), (D) Potential energy contour maps for H_2 at 77 K with the FH effective potential of the inside of the larger pore at different positions along the *c* axis ((1), (2)), with the positions of the Cu(II) ions are denoted in the contour map with a cross. (E), (F) Configurational snapshots of adsorbed H_2 molecules in the framework of CuBOTf obtained from simulations at 77 K and (E) $P = 1$ kPa, (F) $P = 100$ kPa.

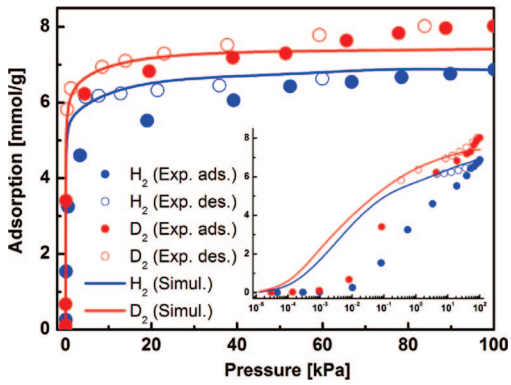

Figure 4. Simulated and experimental adsorption isotherms of CuBOTf for H_2 and D_2 at 40 K. The circles represent the experimental adsorption and desorption isotherm, while the lines represent the simulated isotherms from the CuBOTf model. The relative pressures are given in linear (inset is in logarithmic) scales.

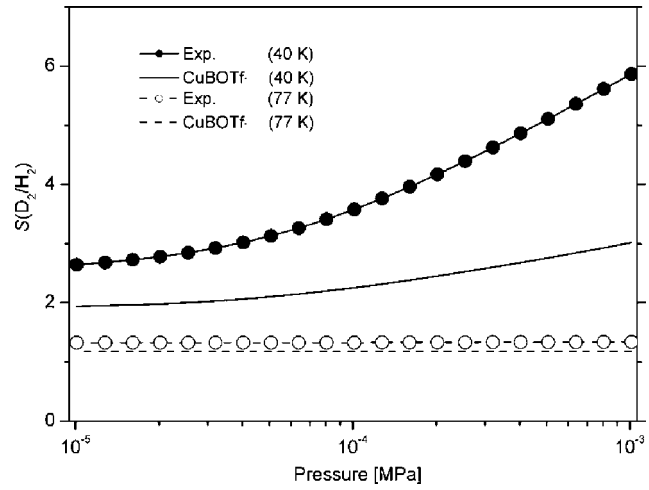

Figure 5. $S(D_2/H_2)$ in CuBOTf calculated by IAST over the pressure range 10^{-5} to 10^{-3} MPa at 77 and 40 K. Experimental values are shown in circles with line, and simulated values from CuBOTf model are shown in lines.

We have applied IAST to the present single-component isotherms from experiments and simulations for the CuBOTf model to predict selectivities of D_2 over H_2 at 40 and 77 K in the pressure range between 0.01 to 1 kPa. The calculation details are given in the Supporting Information. We have assumed a bulk concentration of 0.50 D_2 for mixture adsorption of CuBOTf. The selectivity values (Figure S5, Supporting Information) from simulations at 77 K ($S(D_2/H_2) = 1.3$; corresponds to the 0.57 D_2 in the CuBOTf framework) are in good agreement with those from experiments ($S(D_2/H_2) = 1.2$; 0.55 D_2). In contrast, the selectivity values predicted from simulations at 40 K increase monotonically with pressure ($S(D_2/H_2) = 1.9$ to 3.0; 0.66 to 0.75 D_2), and do not agree quantitatively with the experimental prediction ($S(D_2/H_2) = 2.6$ to 5.8; 0.72 to 0.85 D_2), giving larger selectivity than those from simulations (Figure 5). The reason for this discrepancy should be due to the small effective diameter of a D_2 molecule at 40 K compared with H_2, which is caused by quantum effects. Specifically, D_2 molecules can diffuse into the 1D channels of CuBOTf framework at low pressures more easily than H_2, even though D_2 is heavier than H_2. Therefore, the experimental quasi-equilibrium adsorption of D_2 is larger than that of H_2 at low pressures, resulting in the relatively large selectivity value. The relatively faster diffusion of D_2 than that of H_2 is experimentally evident as described previously. This selectivity $S(D_2/H_2)$ of CuBOTf at 40 K is much higher than the published data of single-wall carbon nanohorns at 77 K. However, the single wall carbon nanohorn has a structure different from single wall carbon nanotube and the predicted selectivity of carbon nanotubes for quantum molecular sieving is sensitive to the interaction potential and rotational-translational coupling.[63] Accordingly, we need the experimental values of the quantum selectivity of carbon nanotube for comparative discussion with MOFs. The selectivity of D_2 over H_2 might be improved if we can exchange linker molecules in the framework for ones with steric influence, which cause a lowering of the diffusivity of quantum H_2 with its larger effective diameter than quantum D_2. The diffusivity of hydrogen

(63) Garberoglio, G.; DeKlavon, M. M.; Johnson, J. K. *J. Phys. Chem. B* **2006**, *110*, 1733–1741.

isotopes below 77 K appears to be an interesting subject for further studies. Adsorption kinetic measurement and quasi-elastic neutron scattering should provide a more clear insight into the dynamic behaviors of adsorbed quantum hydrogen isotopes in MOFs.

Acknowledgment. The synchrotron radiation experiments were performed at SPring-8 with the approval of Japan Synchrotron Radiation Research Institute (JASRI) as a Nanotechnology Support Project of the Ministry of Education, Culture, Sports, Science and Technology (Proposal No. 200 6B1587/BL02B2). This work was supported by the Grant-in-Aid for Scientific Research (Chemistry of Coordination Space) (No. 17036008), Grants-in-Aid for Scientific Research (Grant-in Aid for Young Scientists (B)) (No. 17710091), and Grants-in-Aid for Scientific Research (S) (No. 15101003) by the Japan Society of the Promotion of Science.

Supporting Information Available: Detailed description on materials, adsorption measurement of H_2 and D_2 at low temperature, determination and calculation of isosteric heat of adsorption, calculation method of selectivity of D_2 over H_2, potential parameters for the atoms in CuBOTf framework, X-ray diffraction patterns of CuBOTf samples and the model structures, X-ray diffraction patterns of Cu-BTC, TGA curve of CuBOTf, TGA curve of CuBTC, N_2 adsorption isotherms of CuBOTf at 77 K, experimental H_2 and D_2 adsorption isotherms of Cu-BTC at 77 K, experimental H_2 adsorption isotherms of CuBOTf at 40 K with different equilibration time, and isosteric heats of adsorption for H_2 and D_2. This material is available free of charge via the Internet at http://pubs.acs.org.

JA077469F